C. R. Geoscience 349 (2017) 114–125

Contents lists available at ScienceDirect

Comptes Rendus Geoscience

www.sciencedirect.com

Petrology, Geochemistry

Measuring the surface roughness of geological rock surfaces in SAR data using fractal geometry

Ali Ghafouri [a], Jalal Amini [a,*], Mojtaba Dehmollaian [b], Mohammad Ali Kavoosi [c]

[a] School of Surveying and Geospatial Engineering, Collage of Engineering, University of Tehran, 1439957131 Tehran, Iran
[b] Center of Excellence on Applied Electromagnetic Systems, School of Electrical and Computer Engineering, University of Tehran, 1439957131 Tehran, Iran
[c] Department of Geology, Exploration Directorate of National Iranian Oil Company, 1994814695 Iran

ARTICLE INFO

Article history:
Received 31 March 2017
Accepted after revision 15 April 2017
Available online 22 May 2017

Handled by Isabelle Manighetti

Keywords:
Synthetic Aperture Radar (SAR)
Integral Equation Model (IEM)
Random Fractal Geometry

ABSTRACT

Determining surface morphology using synthetic aperture radar (SAR) data requires accurate topographic and microtopographic models. To distinguish different surface geometric patterns and to differentiate the formation of geological rock surfaces, it is necessary to model the smoothness and roughness of surfaces based on radar signal backscattering. Euclidean geometry is less able than fractal geometry to describe natural phenomena; however, in application to radar backscattering models, fractal geometry has never fully replaced Euclidean geometry. Using fractal geometry only, this paper attempts to improve the backscattering simulation generated by an Integral Equation Model to improve the description of geological rock surfaces. As the application of radar signal backscattering is a rarity in the domain of geology, the paper also discusses the efficiency of the method in improving the results of conventional geological mapping methods. The proposed method is applied to the Anaran geological formation (between Dehloran and Ilam in IRAN) using TerraSAR-X SAR data and in situ roughness measurements on pure sites with rough, intermediate, and smooth morphologies. This implementation shows fractal and diffractal behavior of geological morphologies under various conditions.

1. Introduction

Some geological formations are susceptible to weathering and erosion more so than others, e.g., formations comprising mainly argillaceous limestone and claystone are smoother than pure limestone and dolostone. Formations composed of later lithologies have greater hardness and thus, they are affected little by chemical weathering (Aghanabati, 2004; Candela et al., 2009; Motiei, 1993). Optical image processing methods generally lack the capability to describe and differentiate the morphologies of geometric patterns. Synthetic aperture radar (SAR) data, acquired by airborne and spaceborne sensors, have made it possible to study surface roughness, which provides useful information for geoscientists, particularly geologists. The backscattered signal in all polarizations is affected by surface roughness and it contains surface roughness information (Baghdadi et al., 2015; Gorrab et al., 2015; Martínez-Agirre et al., 2015).

For optimal differentiation of the lithologies of various terrestrial surfaces, it is necessary to consider the smoothness and roughness parameters and to have a description of the type and material of each surface. Spectral images cannot offer such lithological separation for large areas in a cost-effective manner, whereas microwave remote sensing allows lithological separation

* Corresponding author.
E-mail addresses: ali.ghafouri@ut.ac.ir (A. Ghafouri), jamini@ut.ac.ir (J. Amini), m.dehmollaian@ut.ac.ir (M. Dehmollaian), kavoosi@niocexp.ir (M.A. Kavoosi).

http://dx.doi.org/10.1016/j.crte.2017.04.003
1631-0713/

based on the degree of erosion, alteration, and weathering of the surface (Dierking, 1999; Ghafouri et al., 2015; Li et al., 2012).

To measure surface roughness using SAR data, surface geometric parameter(s) must be modeled against the backscattering coefficient for each polarization. Generally, to describe and differentiate patterns and geometric surface textures, it is necessary to model the interaction between the backscattered signals and the surface properties (Ulaby and Long, 2014).

Fung et al. (1992) developed an Integral Equation Model (IEM) as a physically based electromagnetic transfer model that can tolerate a very wide range of roughness dimensions. Theoretically, the IEM is not restricted to any special frequency range or roughness measure (Fung et al., 1992). The IEM exploits rms-height parameters and autocorrelation functions (ACFs) to characterize surface roughness (Hajnsek, 2001).

Given the irregular nature of terrestrial topography and, consequently, the irregular nature of the surface roughness parameters, estimations based on fractal geometry could be contaminated by fewer errors compared with Euclidean geometry. Unlike Euclidean geometrical shapes, fractals are irregular and thus, they are suitable for modeling environmental effects (Falconer, 2005; Franceschetti et al., 1999a; Mandelbrot, 1983).

The main improvements offered by fractal geometry to backscattering modeling, especially the IEM, are as follows:

- application of a generalized (i.e. fractal) ACF instead of Gaussian and exponential ACFs (Baghdadi et al., 2004);
- calculation of the correlation length using fractal parameters (e.g., the fractal dimension) (Zribi et al., 2000). The fractal dimension is the fractal parameter that best describes the complexity of objects and, contrasting with topological dimension, is a real and not a natural number (for linear objects between 1 and 2, and for surfaces between 2 and 3, depending on their levels of complexity);
- computation of the rms-height using fractal parameters (e.g., the fractal dimension) (Franceschetti et al., 1999a);
- calculation and application of the ACF as a function of fractal dimension (Falconer, 2005).

The flowchart presented in Fig. 1 summarizes the proposed method.

Apart from the platform and antenna parameters, the surface parameters, i.e. roughness parameters and dielectric constants, must be measured in situ and extracted, respectively (Fig. 1a). Having two methods of rms-height calculation and three methods of ACF calculation provides six methods of backscattering coefficient simulation via the IEM (Fig. 1b). To evaluate the efficiency of each method, the calculated backscattering coefficients are compared against TerraSAR-X backscattering measurements (Fig. 1c).

The remainder on this paper is organized as follows. Section 2 describes the IEM and the conventional characteristics of geological surface roughness in detail. Furthermore, in this section, we propose the methodology

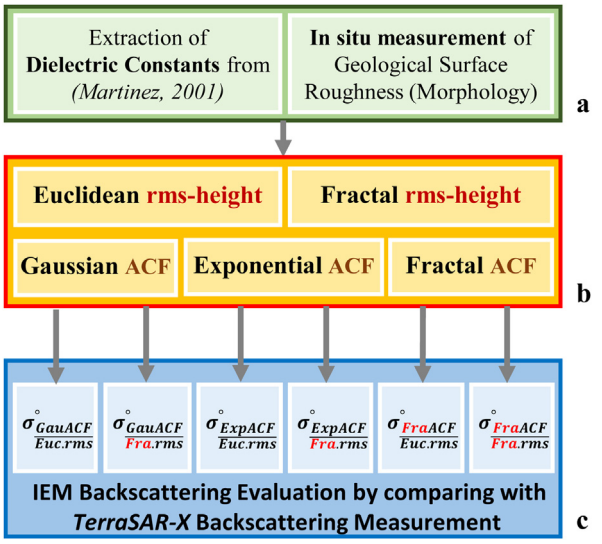

Fig. 1. Study flowchart. For implementation of the IEM, in addition to the platform and antenna parameters, surface parameters as described in (a) are needed. For assessment of the methodology proposed in this paper, surface roughness parameters via six methods of calculation (i.e. six combinations of two rms-height calculations and three ACF calculation methods), mentioned in (b) are inserted into the IEM. To evaluate the results, in (c), they are compared mutually with TerraSAR-X measurements.

of this paper, which is based on using fractal geometry for the IEM input calculation to improve the results. Section 3 describes the study area and the data obtained for the implementation of the methodology and for the comparison with conventional methods. Section 4 presents and compares the results of the implemented simulation of the case study. Section 5 offers concluding remarks, explains the improvements achievable in geological mapping using the IEM model based on surface roughness, and underscores the effectiveness of replacing Euclidean geometry by fractal geometry. Furthermore, the fractal and diffractal regimes of different geological surfaces are analyzed.

2. Microwave Backscattering Model

Fung et al. (1992) introduced the IEM, for which further details were published subsequently by Fung (1994). This model gives the backscattering coefficient σ^{o} in terms of platform, antenna, and surface parameters. Surface parameters involve surface roughness parameters and a dielectric constant. In this paper, the IEM co-polarization equation based on the updated version of the equation is used (Fung and Chen, 2004).

In the following two subsections, the characterizations of surface roughness specifications in both Euclidean and fractal geometries are explained.

2.1. Surface roughness parameters in Euclidean geometry

In backscattering models, surface roughness is characterized via three features: root mean square height (rms-height), correlation length, and ACF.

2.2. Root Mean Square Height (rms-height)

The rms-height, as a statistical parameter, describes the variety of microtopographical elements on the surface. This parameter can be calculated based on a one-dimensional discrete surface profile consisting of N points with elevations h_i (Zribi, 1998).

$$\sigma = \sqrt{\frac{1}{N}\left[\left(\sum_{i=1}^{N} h_i^2\right) - N\bar{h}^2\right]} \tag{1}$$

where

$$\bar{h} = \frac{1}{N}\sum_{i=1}^{N} h_i \tag{2}$$

An increase in the length of the profile usually triggers a rise in the rms-height value (Baghdadi et al., 2006; Baghdadi et al., 2015). Additionally, calculations have shown that in single-scale studies, increasing the measurement profile length affects the rms-height value, but considering fractal geometry, there is no such an effect (Franceschetti et al., 2006).

2.3. Autocorrelation function (ACF)

The ACF defines the extent of the similarities of different parts of a surface. Different parts of rough surfaces, in contrast with smooth surfaces, have less mutual correlation. The normalized ACF, for $\xi = j\Delta x$, where Δx is the spatial resolution of a surface with N samples, is given by:

$$\rho(\xi) = \frac{\sum_{i=1}^{N-j} h_i h_{i+j}}{\sum_{i=1}^{N} h_i^2}. \tag{3}$$

In order to characterize the ACF of a surface fully, the discretization interval, used to sample the profile, should be at least as small as one tenth of the correlation length (Zribi, 1998). In backscattering models, such as the IEM, the surface spectrum is included in the equation. Thus, a regression of Eq. (3) is used to provide a certain equation for the ACF. Two types of regression used commonly are exponential and Gaussian. According to Fernandez-Diaz (2010), the exponential ACF is

$$\rho(\xi) = \mathbf{e}^{-|\xi|/l} \tag{4}$$

and the Gaussian ACF is (Fernandez-Diaz, 2010)

$$\rho(\xi) = \mathbf{e}^{-\xi^2/l^2}, \tag{5}$$

where l is the correlation length. In addition to rms-height, both exponential and Gaussian regressions are suitable to represent roughness geometry in the IEM. According to Hajnsek (2001), the behavior of ACFs for rough surfaces tends to be Gaussian, whereas it tends to be exponential for smooth surfaces. In the calculation of ACFs, correlation length is considered as one third of the semivariogram range (Western et al., 1998).

2.4. IEM modification using fractal geometry

Although not exactly self-similar, natural features are generally self-similar statistically. It means that every part of their structure has statistical properties (i.e. a mean and a standard deviation) similar to those of the entire structure. Regular curves and smooth surfaces can be described using Euclidean geometry, whereas natural features such as clouds, coastlines, and mountains have irregular structures and they should be best described using fractal geometry (Mandelbrot, 1983).

Based on the self-affine fractals definition, we can obtain the following equation between the increments ξ and the difference of the function values over these distances

$$E\left[|h(x+\xi) - h(x)|^2\right] = A\|\xi\|^{2H} \tag{6}$$

where A is a constant, $\|\ \|$ is a distance norm, and H is the Hurst exponent, $0 < H < 1$ (Franceschetti et al., 1999b), which can be obtained using the fractal dimension (FD) (Franceschetti et al., 2000)

$$H = 3 - FD \tag{7}$$

Larger Hurst exponent values have smaller fractal dimensions and indicate smoother surfaces. In the following, we describe the methodologies considered to calculate the input geometric parameters of the IEM necessary to improve the accuracy of surface roughness and geological morphology estimations.

2.5. Computation of rms-height using fractal geometry

For self-affine isotropic stochastic fractal surfaces, the fractal dimension (or, alternatively, the Hurst exponent) and topothesy, together, provide a complete description of the surface. In fractal geometry, there is a relationship between a fractal geometry parameter, called topothesy and rms-height.

Topothesy (T) is a measure of the "strength" of a fractal and it is defined as the horizontal distance between two neighboring points connected by a chord that has one radian of rms-slope (Agnon and Stiassnie, 1991). Using these two fractal parameters (H and T), the standard deviation of the pdf of a fractal surface can be written as

$$\sigma = T^{(1-H)}\tau^H. \tag{8}$$

The standard deviations of the slopes σ_p of the fractal surfaces can be evaluated as σ/τ (Franceschetti et al., 2000):

$$\sigma_{\mathbf{p}} = \left(\frac{T}{\tau}\right)^{1-H}. \tag{9}$$

Therefore, topothesy is the observation scale τ at which the average standard deviation of the slopes is equal to unity. In fact, when $\tau = T$ in Eq. (8), $\sigma = \mathbf{1}$. Topothesy, as well as the Hurst exponent, can be obtained using the fractal dimension (D) and rms-

height (s) (Franceschetti et al., 2000):

$$\begin{cases} D = 3-H \\ s = T^{(1-H)} \end{cases} \tag{10}$$

2.6. Computation of ACFs using fractal geometry

As shown in Eq. (6), the variance of the normal distribution of $\boldsymbol{h}(x+1)-\boldsymbol{h}(x)$ on a fractal surface is $A\xi^{2H}$. Thus, it could be shown that (Zribi et al., 2000):

$$\begin{aligned} E[|\boldsymbol{h}(x+\xi)-\boldsymbol{h}(x)|] &= 2\int_0^{\infty} \frac{u}{\sqrt{A}\xi^H\sqrt{2\pi}} \exp\left(-\frac{u^2}{2A\xi^{2H}}\right) du \\ &= \xi^H \frac{2\sqrt{A}}{\sqrt{2\pi}} \\ &= \xi^H E[|\boldsymbol{h}(x+1)-\boldsymbol{h}(x)|] \end{aligned} \tag{11}$$

where $u = |\boldsymbol{h}(x+\xi)-\boldsymbol{h}(x)|$.

As discussed in Zribi et al. (2000), the fractal autocorrelation function is as follows:

$$\rho(\xi) = \sigma^2\left[1-\frac{1}{2}\left(\frac{\xi}{\tau}\right)^{2H}\right], \tag{12}$$

where $\xi < \tau$, which is valid for scales lower than Δx in which the surface structure is described with the fractal dimension, rms-height, and τ. In Eq. (12), the variance σ^2 is computed from Eq. (8). In Zribi et al. (2000), a good agreement is shown between this function and the exponential function for surfaces that have small values of rms-height, whereas a good agreement is shown with the Gaussian function for surfaces with large values of rms-height.

3. Case study

As a case study to demonstrate the application, the western part of the *Anaran* geological formation was selected. The region is located near Ilam, in western Iran (32°55′–33°05′ N, 46°35′–46°50′ E). In this region, the *Pabdeh* Formation (Paleocene to early Miocene) is superimposed to the *Asmari* Formation (Oligocene to lower Miocene), and the *Asmari* Formation is overlaid conformably by the *Gachsaran* Formation (Lower Miocene) (Aghanabati, 2004; Motiei, 1993). Fig. 2 depicts general views of the outcrop surfaces of these formations.

In this case study, the spectral behaviors of the lithologies have considerable similarities; therefore, the morphologies of the outcrops are considered as the distinguishing constraint (Aghanabati, 2004). Hyperspectral imagery cannot provide textural information of the lithologies (Li et al., 2012). Therefore, discrimination of these units for either geological mapping or interpretation of optical images requires site visits as well as in situ roughness measurements (Dierking, 1999; Lutgens et al., 2014).

The *Asmari* Fm. is composed mainly of limestone in the upper part and of an evaporitic member in the base. Meanwhile, the *Pabdeh* and the *Gachsaran* Fms. comprise marl and argillaceous limestone (Fig. 3a, b). The geomorphology depicted in Fig. 3c is a geological section of *Anaran*. The lower Miocene *Asmari* Fm. as well as the *Gachsaran* and the Paleocene–Oligocene *Pabdeh* Fms. outcrop in the *Anaran* structure. Different outcrop morphologies have different decay properties. The regional lithology contains limestone, dolomite, marl, and anhydride (Aghanabati, 2004).

The *Asmari* and *Pabdeh* Fms. have formed surface outcrops of rock and smooth clay, respectively, while the *Gachsaran* Fm. outcrops represent an intermediate case. Such lithological differences are considered by the different surface roughness parameters in a backscattering electromagnetic model. The dielectric constant is a parameter that, by definition (Fung, 1994), is affected mainly by moisture. If no change is assumed in the value of the dielectric constant, i.e. no change in moisture, differences in surface roughness level will be the only reason for differences in backscattering. This assumption is an acceptable criterion for the discrimination of alteration zones (Lutgens et al., 2014).

The backscattering coefficient is calculated using a TerraSAR-X image, which was acquired in the X-band (i.e. Freq.: 8–12 GHz, wavelength: 3.75–2.50 cm.) in Staring SpotLight mode on an ascending orbit with a 22° incidence angle (Pitz and Miller, 2010). The spatial resolution of the image on the study site is about 25 cm. Regarding signal penetration, according to Pitz and Miller (2010), the backscattered power of the penetrated signal is beyond the dynamic range of the TerraSAR-X antenna; thus, signal penetration is ignored categorically in this study.

Based on the IEM validity range presented by Fung (1994), results of studies by Sahebi et al. (2004), and in situ roughness measurements of the formations in the study

Fig. 2. General view of outcrop surfaces: (a) *Pabdeh* Formation (smooth), (b) *Asmari* Formation (rough), (c) *Gachsaran* Formation (intermediate).

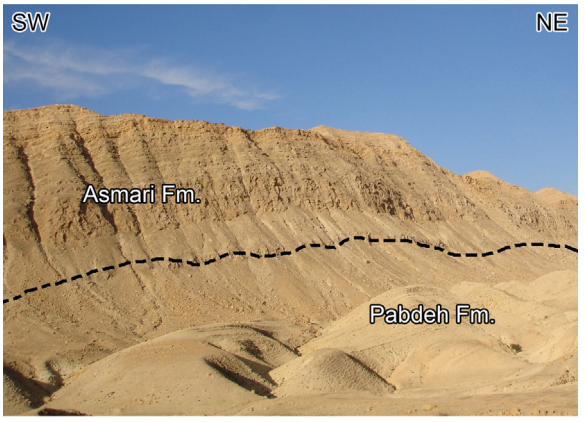

(a)

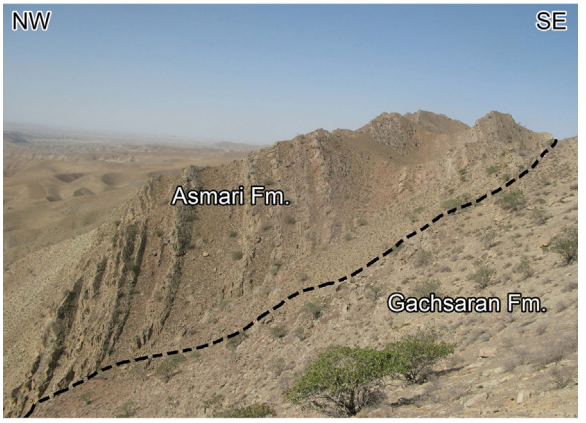

(b)

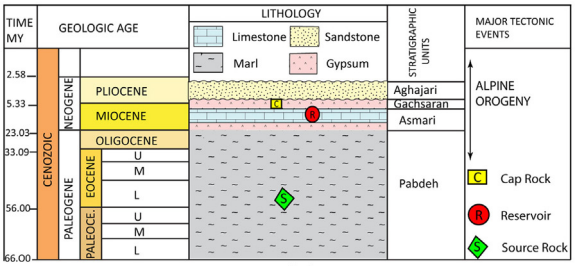

(c)

Fig. 3. (a, b) Field views of the *Asmari*, *Pabdeh*, and *Gachsaran* formations at outcrop sections, (c) stratigraphic chart.

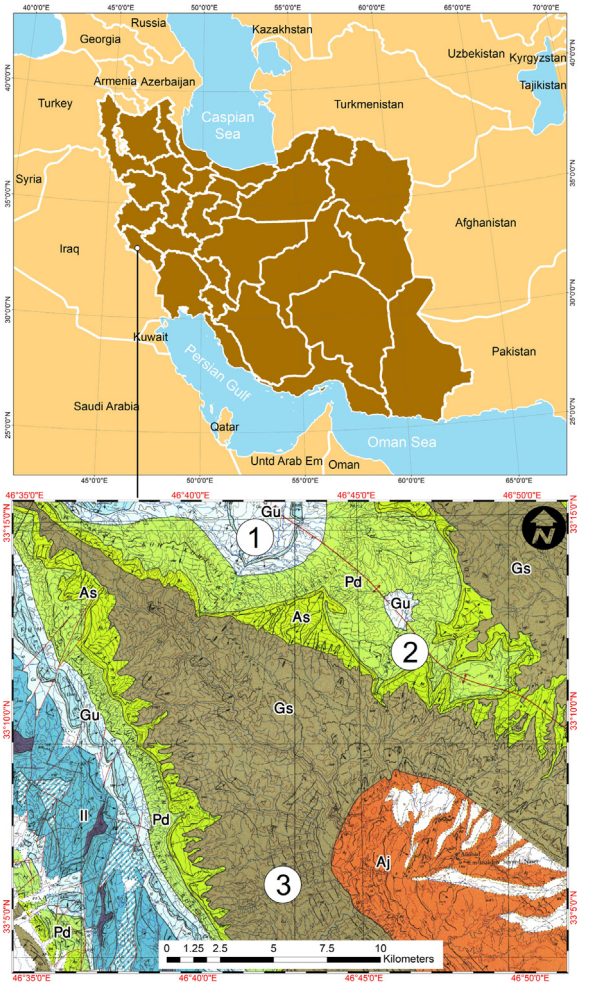

Fig. 4. Case study region in western Iran (upper image). Abbreviations on the geological map (lower image) stand for the geological formations (in alphabetical order): Aj—*Aghajari* Formation (upper Miocene to Pliocene); As—*Asmari* Formation (lower Miocene); Gs—*Gachsaran* Formation (Lower Miocene); Gu—*Gurpi* Formation (Upper Cretaceous); Il—*Ilam* Formation (Upper Cretaceous); Pd—*Pabdeh* Formation (Paleocene to early Paleocene). Site 1, *Pabdeh* Formation (smooth); site 2, *Asmari* Formation (rough), and site 3, *Gachsaran* Formation (an intermediate case between smooth and rough) (Aghanabati, 2004; Motiei, 1993).

region, TerraSAR-X was considered as suitable for this study (Fung, 1994; Sahebi et al., 2004). The morphological details of the study sites are presented in Table Sm1.

As shown schematically in Fig. 4, different sites were selected within the region for the implementation of the proposed method. Despite the mountainous nature of the region, the local slopes at the sites were lower than the error range of the implemented frequency. Each site has different properties in terms of roughness. Site 1 on the *Pabdeh* Fm. has a completely eroded structure, and it appears mostly in the form of soil on the surface. Site 2 is located on the *Asmari* Fm. It has greater resistance against weathering and chemical and physical alteration, and it appears as a rocky face. Site 3 is situated on the *Gachsaran* Fm. and it appears with an intermediate characteristic. Despite the presence of a rocky formation, the site is covered with rock fragments formed via erosion and alteration.

According to the available geological maps of the region, each site is located on a single geological formation, and surface roughness is almost homogenous. These sites were selected inasmuch as they have approximately the same roughness. Moreover, the selection of sites was made to avoid large-scale topography; however, the large-scale DEM of the region was considered to calculate the local incidence angle.

The available geological maps (1:100,000) were those of the National Iranian Oil Company. These maps are able to provide complete information for the different lithologies, and they were used as reference for the alteration zones.

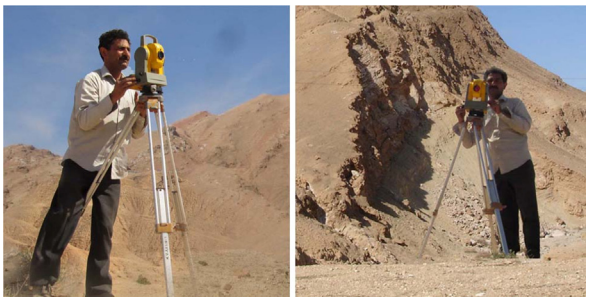

Fig. 5. In situ field measurement using the Total Station surveying equipment (Trimble™5600).

After determining the geologically pure formations, the selection of the sites was performed with consideration of the need for an accessible road to the location of each site.

Surface roughness field measurements were performed using the Total Station surveying equipment (Trimble™5600) and data gathering was undertaken on a grid of points (Fig. 5). This grid at each site comprised a mesh square containing 51×51 points lying in 20×20 m square; i.e. the distance between each pair points was 40 cm. Thus, the DEM of the surface was generated with sampling intervals smaller than the correlation length. As mentioned in the introduction, grid-based data help measure the roughness of any arbitrary profile. Moreover, estimating the fractal dimension for evaluating the correlation function is made possible through the use of a DEM.

After implementing a procedure for wavelet despeckling (Roomi et al., 2011), the backscattering coefficient was calculated based on the product radiometric calibration manual (Pitz and Miller, 2010), and the results are shown in Fig. 6.

In order to georeference the radar data, 18 ground control points (GCPs) were measured using GPS during the site visit for the in situ measurements. Because the climatic

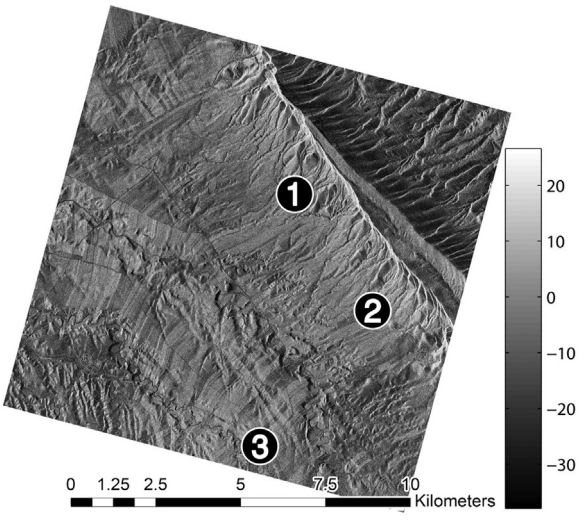

Fig. 6. Evolution of the Sigma Naught coefficient (expressed in dB).

conditions were very dry when the satellite data were acquired, and working on the basis that the geological maps provided the only chance to identify the surface lithologies, no in situ dielectric measurements were performed. All necessary constants were gathered from Martinez and Byrnes (2001).

4. Implementation and analysis of results

By using the IEM equation for *hh* and *vv* polarizations, the values of σ^{o} for all three sites are calculated in six different ways that result from the combination of the three separate modes of calculation of the ACF and the two different methods adopted for the rms-height computation. In other words, Gaussian, exponential, or fractal autocorrelation equations are combined with Euclidean or fractal rms-height evaluations to provide six categories of results.

The dielectric constants were chosen from the tables of Martinez and Byrnes (2001) and, as mentioned in the previous section, the DEMs of the three different sites were obtained using the Total Station surveying instrument. Conventionally, surface roughness measurement is usually performed along one or more linear profiles on the surface. In this study, some zigzag profiles were extracted from the DEMs to calculate the correlation length (l), fractal dimension (FD), and topothesy (T). Such a method of measurement reduces the uncertainty of the parameters considerably, because a long profile can be drawn and interpolated for such a calculation.

The calculation of rms-height was presumed even much more precise. The rms-height, as one of the major parameters of the IEM, was calculated for each cell of the DEM using the eight adjacent cells. The surface parameters of each of the aforementioned sites are tabulated in Table Sm1.

Figs. 7–9, which compare the computed σ^{o} of the IEM, namely the "Simulated IEM" as the results of the six aforementioned ways of calculating the input parameters for 30 randomly selected pixels in each of the study sites, depict the IEM backscattering coefficient values in terms of the measured SAR backscattering coefficient, referred to as the "SAR Measurement" (in dB). Obviously, the proximity of the radar backscattering values (calculated by the IEM model) to the measured values from the SAR image bears testimony to the improvement in the performance of the model.

Fig. 7 shows that the exponential ACF presents better accuracy than the Gaussian function for site 1. In addition, the fractal ACF provides the least deviation of the three. As explained in Section 3, site 1 is located on the *Pabdeh* Fm., which has a corrosive nature, and it is generally found in the form of soil on the surface.

Fig. 8 shows the simulation results of site 2. The Gaussian ACF provides obviously more reliable results than the exponential one. Again, the fractal ACF represents much less deviation than the other two functions. Site 2 is located on the *Asmari* Fm., which is not influenced significantly by physical and chemical erosion and alteration. Generally, its rocky surface is evident.

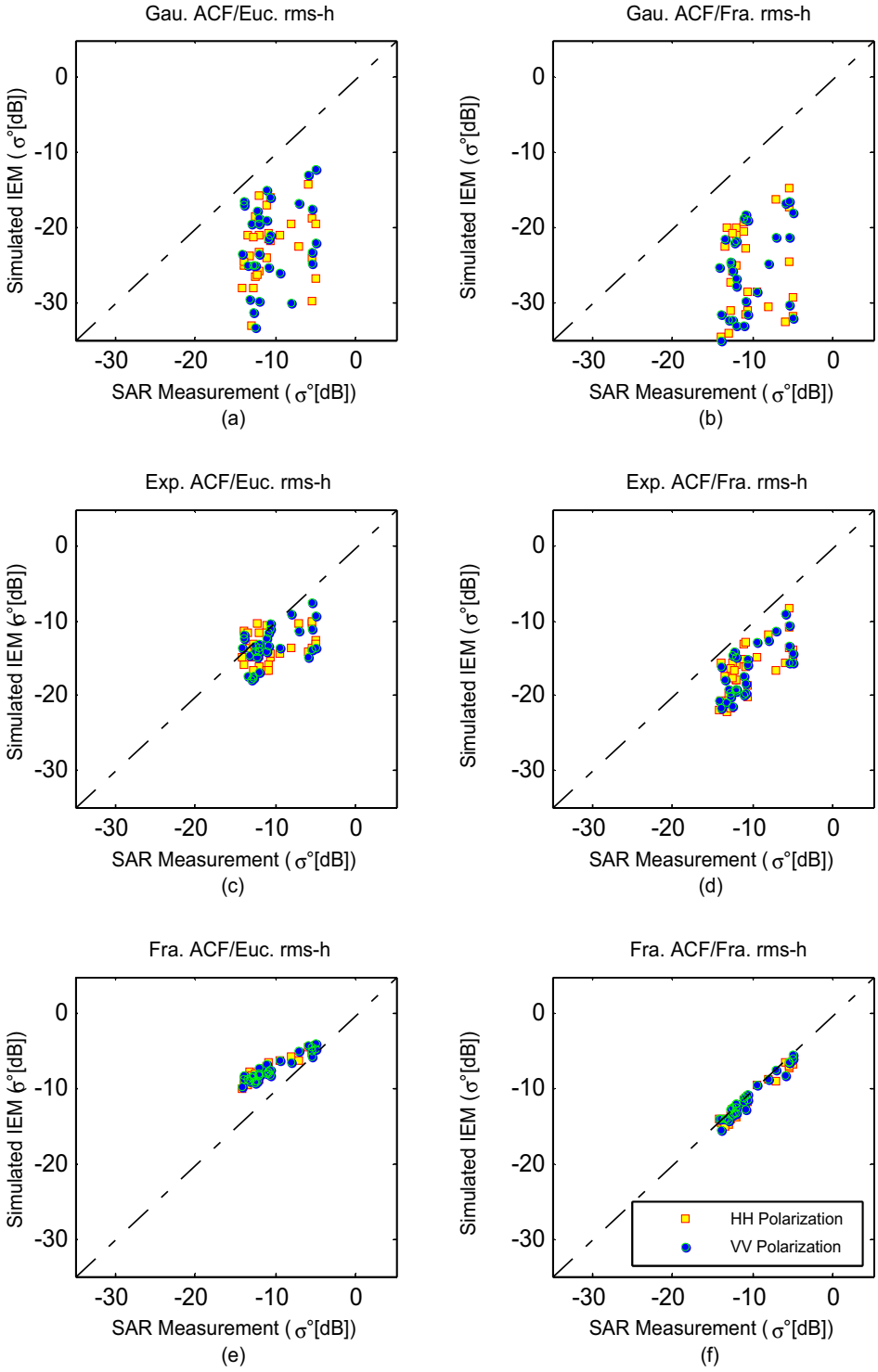

Fig. 7. Backscattering simulation accuracy via the IEM model in two polarizations (*hh* and *vv*) at site 1: (a, b) using Gaussian autocorrelation function with Euclidean and fractal rms-height, (c, d) using exponential autocorrelation function with Euclidean and fractal rms-height, (e, f) using the fractal autocorrelation function with Euclidean and fractal rms-height.

The simulation results of site 3 are shown in Fig. 9. The results of the IEM obtained for this site show a high degree of consistency compared with the other two sites. However, again, the fractal ACF has less unconformity. The site located on the *Gachsaran* Fm. has intermediate roughness. Although it is located amongst rocky regions, the alterations have made its surface somewhat fragmented.

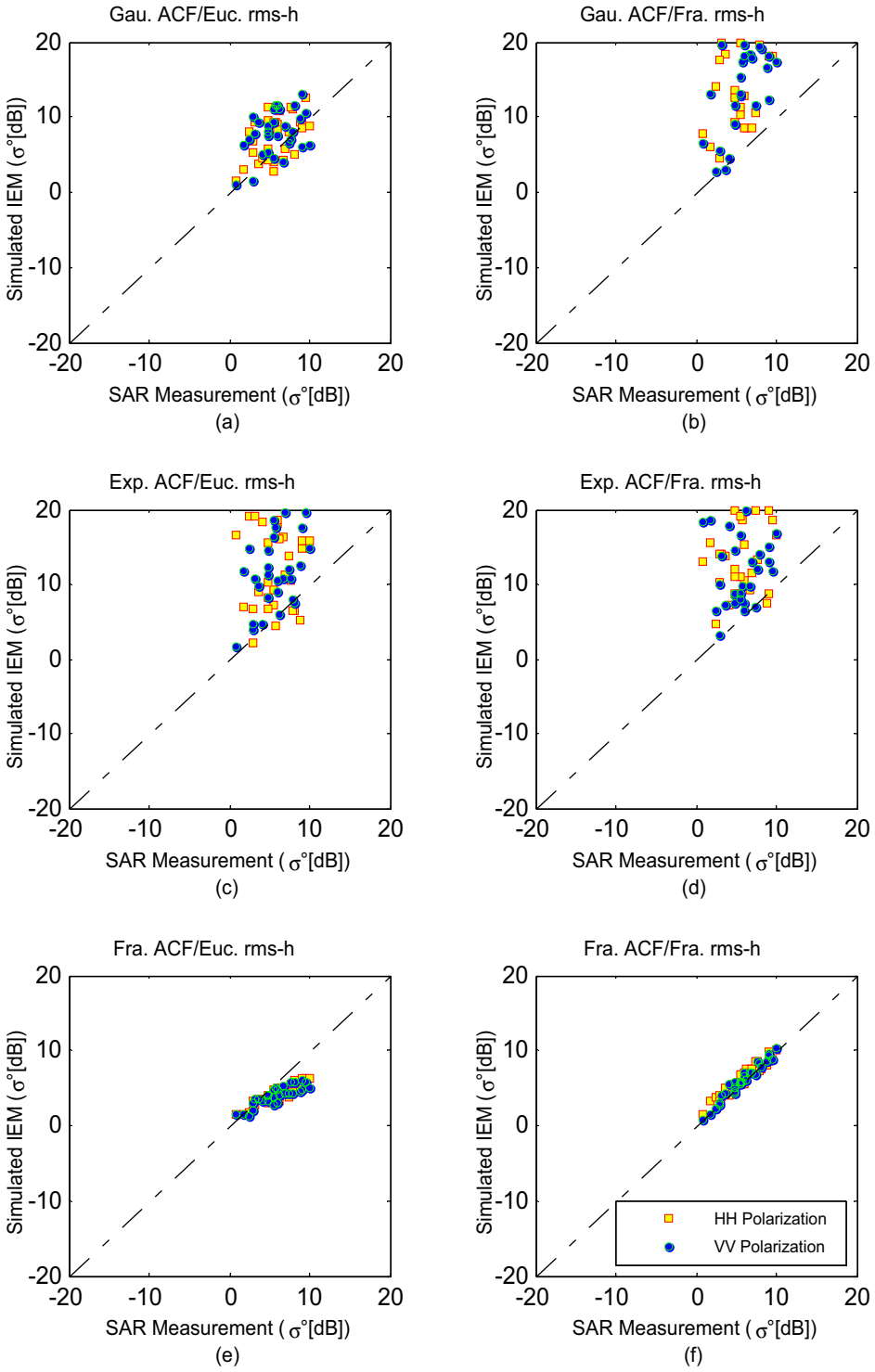

Fig. 8. Backscattering simulation accuracy via the IEM model in two polarizations (*hh* and *vv*) at site 2: (a, b) using Gaussian autocorrelation function with Euclidean and fractal rms-height, (c, d) using exponential autocorrelation function with Euclidean and fractal rms-height, (e, f) using fractal autocorrelation function with Euclidean and fractal rms-height.

Figs. 7–9 depict the effects of each ACF and rms-height. However, a closer inspection is needed to measure the standard deviation of each method numerically. The results for each site and both *hh* and *vv* polarizations are tabulated separately in Table Sm2.

Site 1 has less roughness compared with site 2 and it is modeled more suitably by the exponential function. In

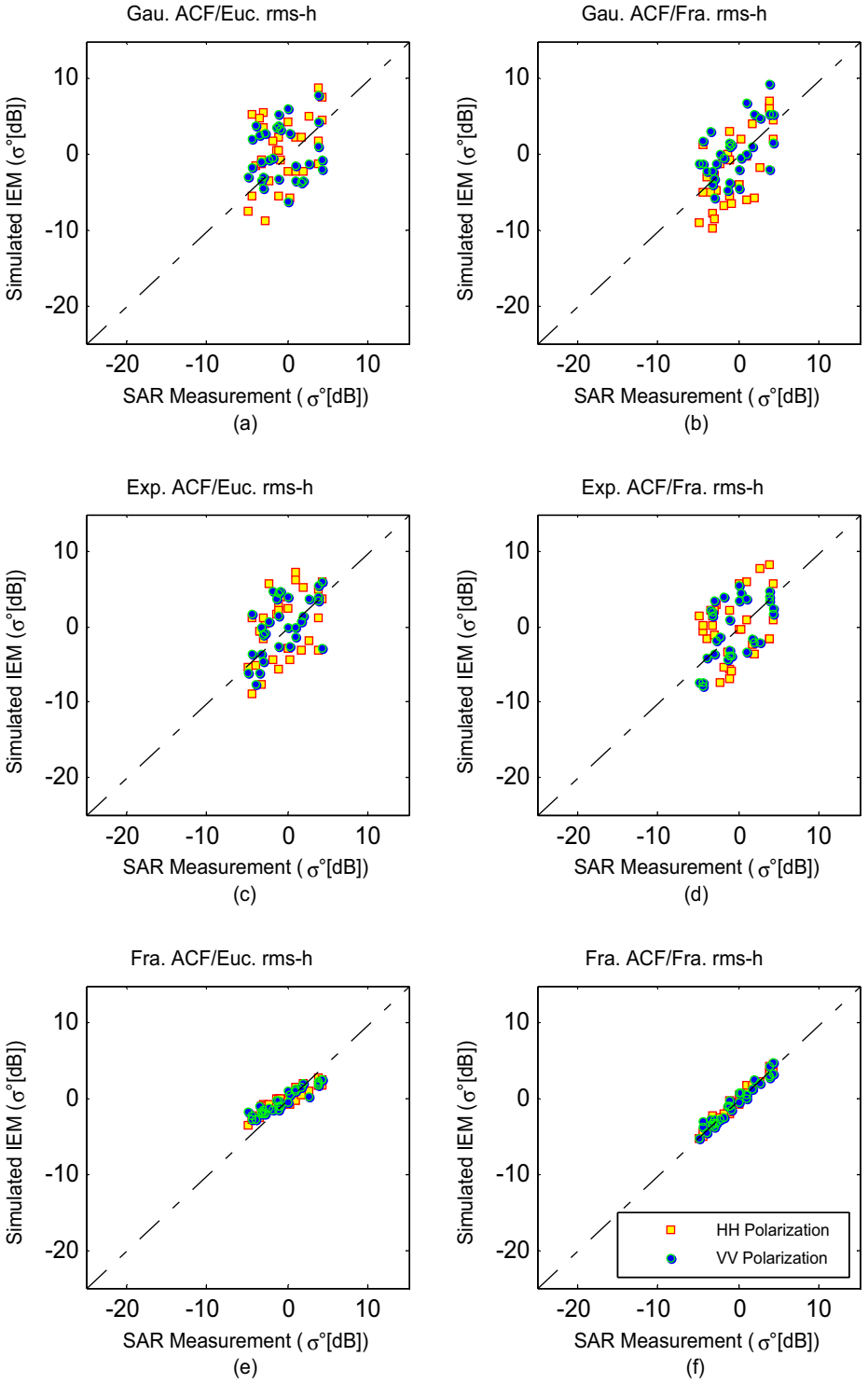

Fig. 9. Backscattering simulation accuracy via the IEM model in two polarizations (*hh* and *vv*) at site 3: (a, b) using Gaussian autocorrelation function with Euclidean and fractal rms-height, (c, d) using exponential autocorrelation function with Euclidean and fractal rms-height, (e, f) using fractal autocorrelation function with Euclidean and fractal rms-height.

addition, it is better to apply the Gaussian ACF for the rough surface of site 2. The effect of rms-height, which is not visually obvious in the previous graphs, can be understood fully from the tabulated data.

Applying Eq. (9), which contains the Hurst exponent and is based on fractal geometry, instead of Eq. (1) generally produces better results, i.e. it reduces the values of the standard deviation. Interestingly, using fractal

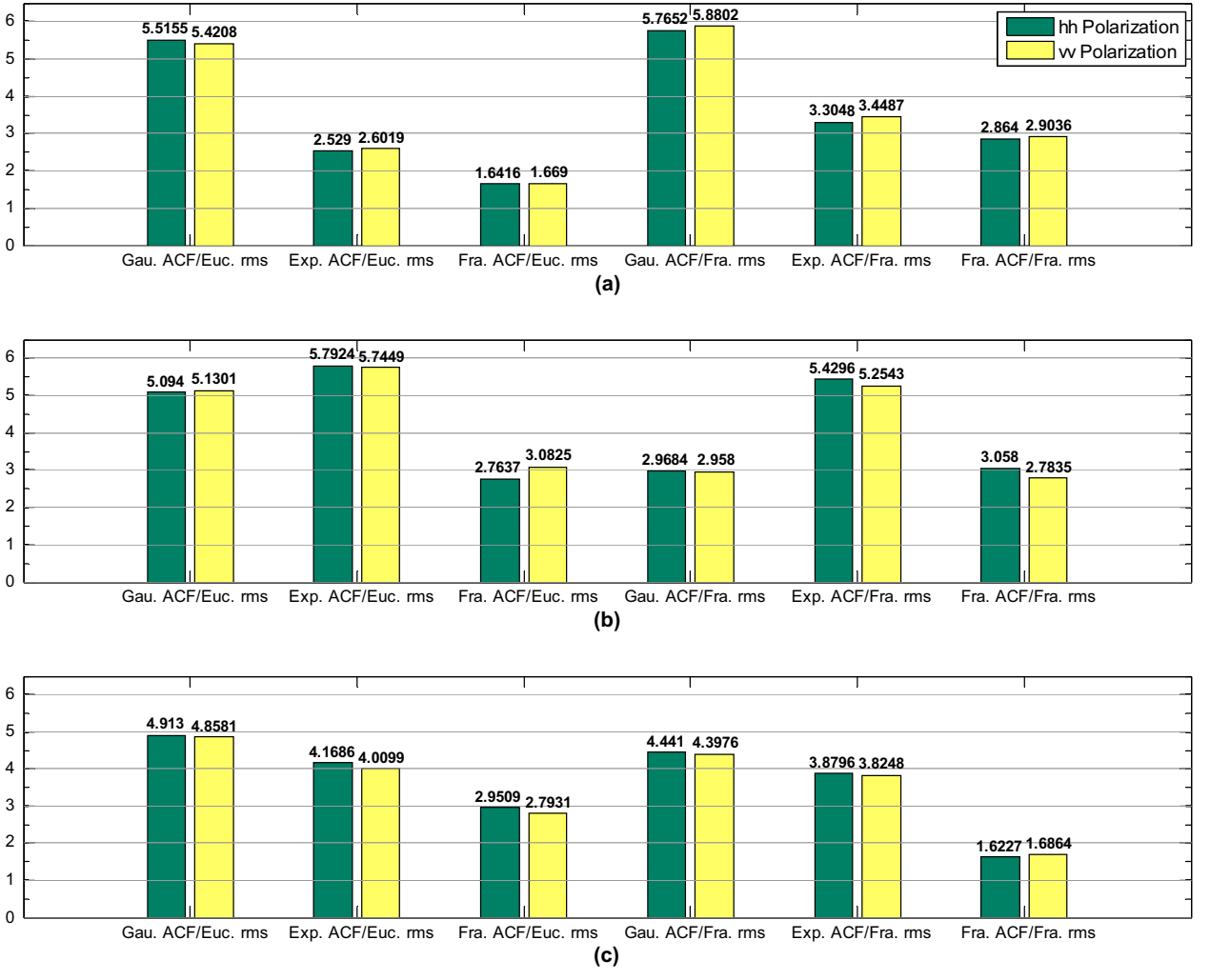

Fig. 10. Standard deviation of calculated backscattering coefficient values via six methods of input calculation, Euclidean and fractal geometries for the geological formations of the study sites for *hh* and *vv* polarizations.

geometry and calculating both the rms-height and the ACF simultaneously results in considerable reduction of the standard deviation. The improvements made in both polarization cases are evident.

The fractal nature of the surface roughness means fractal geometry is more efficient than Euclidean geometry in modeling the surface. Figs. 7–9 show better results for fractal modeling. The values of the standard deviation in Table Sm2, and their illustration on the bar chart of Fig. 10, show the general improvement. However, considering the behaviors of the different geological surfaces with various levels of roughness, we deduce the following:

- there is general similarity in the performance for *hh* and *vv* polarizations and their behaviors have no significant connotation;
- the exponential ACF is much more suitable for smoother surfaces and the Gaussian ACF results are more appropriate for rougher surfaces; however, explicit use of fractal geometry presents the lowest standard deviations;
- rough surfaces offer lower fractal and greater diffractal behavior than smooth or intermediate surfaces.

5. Conclusions

In this paper, a novel method for modeling the surface roughness of geological top formations using SAR polarimetric data was presented, with the aim of improving the precision of geological maps. The basis of this method is random fractal geometry. Because of the irregular and fractal nature of natural surfaces, an electromagnetic backscattering model of radar signals based on fractal geometry, in comparison with Euclidean geometry, for the calculation of geometric input parameters of the IEM, provides much more accurate results, i.e. closer to SAR measured values. Generally, the improvements are clear for both *hh* and *vv* polarizations. Furthermore, the level of improvement was similar for all three of the study sites. However, the improvement for rougher surfaces (site 2) was much more pronounced. Using this method in geological mapping could improve traditional geological mapping processes that conventionally are based on hyperspectral image processing. It must be recognized that roughness modeling cannot be used as a stand-alone mapping methodology; however, it can improve the results of traditional geological mapping methods and reduce the requirements for site visits and field measurement operations considerably.

Acknowledgment

The authors would like to thank the University of Tehran Vice Chancellor for Research for supporting this paper. Furthermore, we would like to acknowledge DLR and the TerraSAR-X program for providing SAR data for the study area. Helpful comments and suggestions regarding the paper given by Dr. Barette and Dr. Ocavalie are acknowledged with gratitude.

Appendix A. Supplementary data

Supplementary data associated with this article can be found, in the online version, at http://dx.doi.org/10.1016/j.crte.2017.04.003.

References

Aghanabati, A., 2004. Geology of Iran. Geological Survey of Iran. Geological Survey & Mineral Explorations of Iran (GSI).
Agnon, Y., Stiassnie, M., 1991. Remote sensing of the roughness of a fractal sea surface. J. Geophys. Res. Oceans 96 (C7), 12773–12779, http://dx.doi.org/10.1029/91JC00903.
Baghdadi, N., Gherboudj, I., Zribi, M., Sahebi, M., King, C., Bonn, F., 2004. Semi-empirical calibration of the IEM backscattering model using radar images and moisture and roughness field measurements. Int. J. Remote Sensing 25 (18), 3593–3623, http://dx.doi.org/10.1080/01431160310001654392.
Baghdadi, N., Holah, N., Zribi, M., 2006. Calibration of the Integral Equation Model for SAR data in C-band and HH and VV polarizations. Int. J. Remote Sens. 27 (4), 805–816, http://dx.doi.org/10.1080/01431160500212278.
Baghdadi, N., Zribi, M., Paloscia, S., Verhoest, N., Lievens, E.C., Baup, H., Mattia, F.F., 2015. Semi-empirical calibration of the Integral Equation Model for co-polarized L-band backscattering. Remote Sens. 7 (10), 13626–13640.
Candela, T., Renard, F., Bouchon, M., Brouste, A., Marsan, D., Schmittbuhl, J., Voisin, V., 2009. Characterization of fault roughness at various scales: Implications of three-dimensional high resolution topography measurements. Pure Appl. Geophys. 166 (10–11), 1817–1851.
Dierking, W., 1999. Quantitative roughness characterization of geological surfaces and implications for radar signature analysis. IEEE Trans. Geosci. Remote Sens. 37 (5), 2397–2412.
Falconer, K., 2005. Random Fractals. In: Fractal Geometry. John Wiley & Sons, Ltd, 244–257.
Fernandez-Diaz, J.C., 2010. Characterization of surface roughness of bare agricultural soils using LiDAR. University of Florida, Gainesville, FL, USA.
Franceschetti, G., Iodice, A., Maddaluno, S., Riccio, D., 2000. A fractal-based theoretical framework for retrieval of surface parameters from electromagnetic backscattering data. IEEE Trans. Geosci. Remote Sens. 38 (2), 641–650.
Franceschetti, G., Iodice, A., Migliaccio, M., Riccio, D., 1999a. Fractals and the small perturbation scattering model. Radio Science 34 (5), 1043–1054.
Franceschetti, G., Iodice, A., Migliaccio, M., Riccio, D., 1999b. Scattering from natural rough surfaces modeled by fractional Brownian motion two-dimensional processes. IEEE Trans. Antennas Propag. 47 (9), 1405–1415.
Franceschetti, G., Iodice, A., Perna, S., Riccio, D., 2006. Efficient simulation of airborne SAR raw data of extended scenes. IEEE Trans. Geosci. Remote Sens. 44 (10), 2851–2860.
Fung, A.K., 1994. Microwave Scattering and Emission Models and Their Applications. Artech House.
Fung, A.K., Chen, K.S., 2004. An update on the IEM surface backscattering model. IEEE Geosci. Remote Sens. Lett. 1 (2), 75–77, http://dx.doi.org/10.1109/LGRS.2004.826564.
Fung, A.K., Li, Z., Chen, K.S., 1992. Backscattering from a randomly rough dielectric surface. IEEE Trans. Geosci. Remote Sens. 30 (2), 356–369.
Ghafouri, A., Amini, J., Dehmollaian, M., Kavoosi, M., 2015. Random fractals geometry in surface roughness modeling of geological formations using synthetic aperture radar images. J. Geomatics Sci. Technol. 5 (2), 97–108.
Gorrab, A., Zribi, M., Baghdadi, N., Mougenot, B., Chabaane, Z.L., 2015. Potential of X-band TerraSAR-X and COSMO-SkyMed SAR data for the assessment of physical soil parameters. Remote Sens. 7 (1), 747–766.
Hajnsek, I., 2001. Inversion of surface parameters using polarimetric SAR. Friedrich-Schiller-Universität, Jena, Germany.
Li, Z., Yang, R., Dang, F., Peijun Du, P., Zhang, X., Tan, B., Zhao, H., Su, H., 2012.In: A review on the geological applications of hyperspectral remote sensing technology, Paper presented at the 4th Workshop on Hyperspectral Image and Signal Processing: Evolution in Remote Sensing (WHISPERS), 4-7 June 2012.
Lutgens, F.K., Tarbuck, E.J., Tasa, D., 2014. Essentials of geology. Pearson new international edition.
Mandelbrot, B.B., 1983. The fractal geometry of nature, 173. Macmillan.

Martínez-Agirre, A., Álvarez-Mozos, J., Lievens, H., Verhoest, N., Giménez, E.C.R., 2015.In: Sensitivity of C-band backscatter to surface roughness parameters measured at different scales, Paper presented at the 2015 IEEE International Geoscience and Remote Sensing Symposium (IGARSS).

Martinez, A., Byrnes, A.P., 2001. Modeling dielectric-constant values of geologic materials: An aid to ground-penetrating radar data collection and interpretation. Kansas Geological Survey, University of Kansas, KS, USA.

Motiei, H., 1993. Stratigraphy of Zagros. Treatise on the Geology of Iran (1) Geological Survey & Mineral Explorations of Iran (GSI), 60–151.

Pitz, W., Miller, D., 2010. The TerraSAR-X Satellite. IEEE Trans. Geosci. Remote Sens. 48 (2), 615–622.

Roomi, S., Kalaiyarasi, D., Kasturi Rangan, N., 2011.In: Discrete wavelet transform based despeckling for SAR images, In: Proc. 2011 World Congress on Information and Communication Technologies (WICT), Mumbai, India, 11-14 Dec. 2011.

Sahebi, M.R., Bonn, F., Bénié, G.B., 2004. Neural networks for the inversion of soil surface parameters from synthetic aperture radar satellite data. Can. J. Civil Eng. 31 (1), 95–108.

Ulaby, F.T., Long, D.G., 2014. Microwave Radar and Radiometric Remote Sensing. University of Michigan Press, Ann Arbor, pp. 425–445.

Western, A.W., Bloschl, G., Grayson, R.B., 1998. How well do indicator variograms capture the spatial connectivity of soil moisture? Hydrol. Process. 12 (12), 1851–1868.

Zribi, M., Ciarletti, V., Taconet, O., Paillé, J., Boissard, P., 2000. Characterisation of the soil structure and microwave backscattering based on numerical three-dimensional surface representation: Analysis with a fractional Brownian model. Remote Sens. Environ. 72 (2), 159–169.

Zribi, M., 1998. Développement de nouvelles méthodes de modélisation de la rugosité pour la rétrodiffusion hyperfréquence de la surface du sol. Télédétection : Traitement du signal. Ph.D. thesis, Université Paul-Sabatier, Toulouse, France.